

Detecting the Dusty Debris of Terrestrial Planet Formation

Scott J. Kenyon

Smithsonian Astrophysical Observatory, 60 Garden Street, Cambridge, MA 02138, USA;
e-mail: skenyon@cfa.harvard.edu

and

Benjamin C. Bromley

Department of Physics, University of Utah, 201 JFB, Salt Lake City, UT 84112, USA;
e-mail: bromley@physics.utah.edu

ABSTRACT

We use a multiannulus accretion code to investigate debris disks in the terrestrial zone, at 0.7–1.3 AU around a $1 M_{\odot}$ star. Terrestrial planet formation produces a bright dusty ring of debris with a lifetime of $\gtrsim 10^6$ yr. The early phases of terrestrial planet formation are observable with current facilities; the late stages require more advanced instruments with adaptive optics.

Subject headings: planetary systems – solar system: formation – stars: formation – circumstellar matter

1. INTRODUCTION

Stars are born with circumstellar disks. Young stars have opaque, gaseous disks with radii of 100–1000 AU and masses of 0.001–0.1 M_{\odot} (e.g. Wyatt, Dent, & Greaves 2003). The disks absorb and re-emit light from the central star and generate internal energy by viscous dissipation (e.g., Lynden-Bell & Pringle 1974; Adams, Lada, & Shu 1987; Kenyon & Hartmann 1987; Bertout, Basri, & Bouvier 1988; Chiang & Goldreich 1999). Typical disk temperatures range from ~ 2000 K at the inner edge to ~ 30 – 50 K at the outer edge. Because the disk is cooler than the star, it produces an infrared (IR) excess of radiation compared to a normal stellar photosphere. The excess is ~ 1 mag at $3.5 \mu\text{m}$ (L-band), 2–5 mag at $10 \mu\text{m}$ (N-band), and 8–10 mag at $100 \mu\text{m}$ (e.g., Kenyon & Hartmann 1995).

As they age, stars lose their disks. The fraction of stars with opaque disks declines from 80%–90% for 1 Myr old stars to 10%–20% for 10 Myr old stars (Haisch, Lada, & Lada

2001b). Stars older than 10 Myr rarely have opaque disks. However, many older stars have optically thin, ‘debris disks,’ with radii of 100–1000 AU and masses of 0.01–10 M_{\oplus} (e.g., Habing et al. 2001; Spangler et al. 2001; Greaves & Wyatt 2003). Debris disks are cooler than opaque disks and emit most of their radiation at wavelengths, $\lambda \gtrsim 10 \mu\text{m}$ (e.g., Lagrange et al. 2000).

Recent observations suggest a rapid evolution from opaque disk to debris disk. In the Taurus-Auriga cloud, many young stars have the mid-IR colors of an opaque disk, $K-L \sim 1$, $K-N \gtrsim 2$; others have the colors of cool main-sequence stars, $K-L \lesssim 0.4$, $K-N \lesssim 0.5$ (Kenyon & Hartmann 1995; Hartigan et al. 1990). Only $\sim 1\%$ – 2% of the 1–3 Myr old stars in this cloud have intermediate colors. Other nearby star-forming regions have similar fractions of ‘transition’ disks (e.g. Bontemps et al. 2001; Haisch et al. 2001a; Jayawardhana et al. 2001; Stassun et al. 2001; Najita, Carr, & Mathieu 2003), suggesting a transition timescale of $\lesssim 10^5$ yr for material at 0.1–3 AU.

The transformation from opaque disk to debris disk requires the ‘disappearance’ of ~ 0.001 – $0.1 M_{\odot}$ of gas and dust. Planet formation plausibly explains this evolution. In the planetesimal model, dust grains grow to mm sizes and fall into the disk midplane. The grains evolve into 1 km ‘planetesimals’ (Goldreich & Ward 1973; Weidenschilling & Cuzzi 1993; Youdin & Shu 2003), which collide and merge into planets (e.g. Lissauer 1993; Wetherill & Stewart 1993; Kenyon & Luu 1999). The gravity of 1000 km or larger planets stirs up leftover planetesimals to large velocities; a cascade of collisions then removes most of the solid material remaining in small objects (Williams & Wetherill 1994). At the same time, accretion, photoevaporation, disk and stellar winds, and perhaps other processes remove the gas (e.g. Hollenbach et al. 1994; Pollack et al. 1996; Konigl & Pudritz 2000).

Recent studies support this picture. Observations suggest grain growth in the disks surrounding the youngest stars (e.g. D’Alessio, Calvet, & Hartmann 2001; Throop et al. 2001; Hogerheijde et al. 2003; van Boekel et al. 2003). Vortices and other density fluctuations in the disk promote the growth of grains into planetesimals (Adams & Watkins 1995; Supulver & Lin 2000; Haghighipour & Boss 2003). At ~ 0.3 – 3 AU, rocky planetesimals merge and grow into planets in 1–10 Myr (Wetherill & Stewart 1993; Weidenschilling et al. 1997; Chambers 2001). At 10–50 AU, icy planetesimals become planets in 10–30 Myr (Kenyon & Luu 1999). Once icy planets form, a collisional cascade explains the luminosities, structures, and timescales of debris disks (Dominik & Decin 2004; Kenyon et al. 1999; Kenyon & Bromley 2002b, 2004).

Here, we consider the formation of terrestrial planets and debris disks. A collisional cascade associated with the formation of 2000 km and larger rocky planets produces measurable IR excesses which last for $\sim 10^6$ yr, comparable to transition times observed in pre-main–

sequence stars. The early stages of terrestrial planet formation are observable with current facilities. The final accumulation phases require more sensitive instruments with adaptive optics.

We outline the model in §2, describe the calculations in §3, and conclude with a brief discussion in §4.

2. THE MODEL

We adopt the Safronov (1969) statistical approach to calculate the collisional evolution of an ensemble of planetesimals in orbit around a star of mass M_\odot and luminosity L_\odot (Kenyon & Bromley 2002a, 2004). The model grid contains N concentric annuli with widths δa_i centered at heliocentric distances a_i . Calculations begin with a differential mass distribution $n(m_{ik})$ of bodies with orbital eccentricity $e_{ik}(t)$ and inclination $i_{ik}(t)$.

To evolve the mass and velocity distributions in time, we solve the coagulation and Fokker-Planck equations for bodies undergoing inelastic collisions, drag forces, and long-range gravitational interactions (Kenyon & Bromley 2002a). We adopt collision rates from kinetic theory and use an energy-scaling algorithm to assign collision outcomes (Wetherill & Stewart 1993; Weidenschilling et al. 1997; Davis et al. 1985). To compute collision rates and outcomes between planetesimals in different annuli, we derive an overlap region whose size depends on the eccentricities and masses of the planetesimals in each annulus (Kenyon & Bromley 2002a, Appendix A). We derive changes in orbital parameters from gas drag, dynamical friction, and viscous stirring (Adachi et al. 1976; Ohtsuki, Stewart, & Ida 2002). Our approach does not include tidal interactions between the largest bodies and the gas (e.g. Agnor & Ward 2002) or the largest bodies and smaller planetesimals (Rafikov 2001, 2003). Our tests show that these effects are small for the early evolution discussed here, but become important at later stages when the largest bodies merge into planets. We plan to discuss these issues in future papers. Kenyon & Bromley (2001, 2002a) summarize algorithms and tests of the code (see also Kenyon & Luu 1998, 1999).

To compute dust masses and luminosities, we use dust production rates and particle scale heights derived from the multiannulus coagulation code as input to a separate dust evolution code (Kenyon & Bromley 2004). This second calculation includes collisions among dust grains along with gas and Poynting-Robertson drag. Because collision timescales are shorter than timescales for gas and radiation drag, collisions set the size distribution for small grains and the total optical depth through the disk. We use a simple radiative transfer method to derive the optical depth through the disk; dust luminosities follow from the dust

scale height. To derive dust temperatures, we assume grains have an albedo of 20% and emit as blackbodies in radiative equilibrium.

3. CALCULATIONS

Our numerical calculations begin with 1–1000 m planetesimals in 32 concentric annuli centered at a distance of 1 AU from the Sun. We consider (i) thin torus calculations at 0.84–1.16 AU with $\delta a_i = 0.01$ and (ii) thick torus calculations at 0.68–1.32 AU with $\delta a_i = 0.02$. The planetesimals have an initial surface density $\Sigma = \Sigma_0 (a/1 \text{ AU})^{-3/2}$. We consider models with $\Sigma_0 = 8, 16,$ and 32 g cm^{-2} . The ‘minimum mass solar nebula’ has $\Sigma_0 \sim 16 \text{ g cm}^{-2}$ (Weidenschilling 1977; Hayashi 1981). In each annulus, the initial mass distribution has 30–60 mass batches, with a mass spacing, $\delta = m_{i+1}/m_i = 1.4\text{--}2.0$, between successive batches. The cumulative number of bodies is $N_C \propto m_i^{-0.03}$. We add mass batches as planetesimals grow in mass. Each planetesimal batch begins in a nearly circular orbit with eccentricity $e_0 = 10^{-4}$ and inclination $i_0 = e_0/2$. The initial gas density at 1 AU is $\rho_g = 1.07 \times 10^{-9} (\Sigma_0/16 \text{ g cm}^{-2}) \text{ g cm}^{-3}$; Kenyon & Bromley (2002a) describe how we scale the gas density with radius and time. For fragmentation parameters, we adopt a tensile strength in the range $S_0 = 10^6\text{--}10^8 \text{ erg g}^{-1}$ and a crushing energy $Q_c = 10^7\text{--}10^9 \text{ erg g}^{-1}$ (Davis et al. 1985; Wetherill & Stewart 1993).

In our calculations, the growth of planetesimals into planets follows a standard pattern (Lissauer 1993; Wetherill & Stewart 1993; Weidenschilling et al. 1997). At 1 AU, it takes 500–1000 yr for 1 km objects to grow into 100 km objects. Collisions produce a small amount of debris, which adds material to the mass batches for 1–100 m objects. Gas drag circularizes the orbits of small objects and removes $\sim 0.001\%$ of this mass from the innermost annuli. Viscous stirring raises the eccentricities of the 0.1–10 km objects; dynamical friction lowers the eccentricities of larger objects. Gravitational focusing factors increase and runaway growth begins.

Runaway growth concentrates most of the mass in the largest objects. It takes $\sim 1 - 2 \times 10^4$ yr to produce 1000 km objects and another $\sim 1 - 2 \times 10^4$ yr to produce 2000 km objects. During runaway growth, viscous stirring raises the velocities of 100 m to 10 km bodies to the disruption limit. Collisions among these bodies then produce substantial debris instead of mergers. Continued stirring lowers gravitational focusing factors and retards the growth of the largest objects. As large objects grow slowly, erosive collisions reduce the number of 100 m to 10 km objects substantially.

Figure 1 shows two snapshots of the mass distribution for large objects in a thin torus

calculation. During the first 10^5 yr, protoplanets form in the inner annuli. As the collisional cascade begins at ~ 0.9 AU, protoplanets start to form at ~ 1.1 AU. Smaller gravitational focusing factors and depletion by erosive collisions then limit growth. By $\sim 10^6$ yr, planet growth saturates at radii ~ 3000 km. A few protoplanets each with masses of 0.01 – $0.1 M_{\oplus}$ then contain $\gtrsim 70\%$ of the remaining mass (25%–50% of the initial mass). The large eccentricities of these protoplanets allow their orbits to cross; multiple orbit-crossings lead to mergers and the formation of Earth-like planets (Chambers 2001). Because our coagulation code does not treat these interactions accurately, we stopped our calculations at ~ 2 Myr. We plan to report on calculations that incorporate an n -body code in future papers (Bromley & Kenyon 2004).

Figure 2 shows the evolution of the dust mass for models with Wetherill & Stewart (1993) fragmentation. We divide the debris into small grains with sizes of 1 – $1000 \mu\text{m}$ and large particles with sizes of 1 – 1000 mm. At the start of these calculations, collisions yield mergers with little dust. As larger objects form, their gravity stirs up planetesimals to the disruption velocity. Dust production grows rapidly. The dust mass peaks when the largest objects have radii of ~ 2000 km. Because the growth time varies inversely with the initial mass in planetesimals, more massive disks reach peak dust mass before less massive disks. More massive disks also produce more dust. We derive a simple relation for the dust mass as a function of initial surface density and time:

$$M_{S/L} \approx M_{S/L,0} \left(\frac{\Sigma_0}{16 \text{ g cm}^{-2}} \right) \left(\frac{t_0}{t} \right) \quad \text{for } t \gtrsim t_0, \quad (1)$$

where $M_{S,0} \sim 10^{23}$ g for small particles, $M_{L,0} \sim 3 \times 10^{24}$ g for large particles, and $t_0 \sim 10^5$ yr. This relation is fairly independent of the fragmentation algorithm and the material properties of the planetesimals (Kenyon & Bromley 2001; Dominik & Decin 2004).

Despite the rapid decline in dust mass, dust in the terrestrial zone produces an observable IR excess. Figure 3 illustrates the evolution of the $10 \mu\text{m}$ and $20 \mu\text{m}$ excesses relative to a normal stellar photosphere for models with Wetherill & Stewart (1993) fragmentation. The IR excesses peak when the dust mass reaches its maximum. The largest planets then have radii of 2000 km. As planets grow to sizes of 3000 km and larger, IR excesses decline considerably. The 0.01 – $0.1 M_{\oplus}$ objects then collide and merge into Earth-like planets (Chambers 2001; Bromley & Kenyon 2004). During this final accumulation phase, 10 – $20 \mu\text{m}$ excesses are small.

As the 10 – $20 \mu\text{m}$ excesses decline, individual collisions among 10 – 100 km objects produce fluctuations in the dust production rate. These disruptive collisions yield large variations in the 10 – $20 \mu\text{m}$ excesses.

Infrared excesses are relatively insensitive to the size of the zone where terrestrial planets

form. In the left panels of Figure 3, calculations in a thin torus at 0.84–1.16 AU produce excesses of ~ 1 –2 mag at $10\ \mu\text{m}$ and ~ 3 mag at $20\ \mu\text{m}$. Calculations in a larger torus yield somewhat larger excesses (Figure 3; right panels). We estimate that a complete calculation of the terrestrial zone at 0.3–3 AU would yield 10 – $20\ \mu\text{m}$ excesses $\lesssim 1$ mag larger than the excesses in Figure 3.

Our calculations indicate that the magnitude of the 10 – $20\ \mu\text{m}$ excess produced by terrestrial dust is insensitive to many model parameters. Because collisions dominate the destruction of planetesimals and dust grains, the details of gas and Poynting-Robertson drag are unimportant. Rapid early growth erases the initial size distribution; variations in the slope of the initial power-law size distribution do not modify the results. Changes in the fragmentation parameters S_0 and Q_c produce modest, $\sim 25\%$, changes in the dust production rates and the growth timescales. As noted in previous studies, Davis et al. (1985) fragmentation yields shorter growth times and smaller dust production rates; this algorithm also concentrates a larger fraction of the initial mass into the largest bodies. However, the long-term evolution of the IR excesses in models with Davis et al. (1985) fragmentation is nearly identical to the evolution with Wetherill & Stewart (1993) fragmentation (Kenyon & Bromley 2004).

The initial mass in planetesimals controls the timescale of the dust evolution. Massive disks produce larger planets more rapidly than low mass disks. The timescale for the formation of 2000 – 3000 km planets scales inversely with the mass (Lissauer 1987; Wetherill & Stewart 1993; Weidenschilling et al. 1997; Kenyon & Luu 1998, 1999), $t_P \approx 1 - 2 \times 10^5$ yr ($16\ \text{g cm}^{-2}/\Sigma_0$).

The initial surface density also sets the geometry of the dusty disk. In calculations with $\Sigma_0 \gtrsim 16\ \text{g cm}^{-2}$, the radial optical depth of the disk often exceeds unity. The opaque, inner disk can then shadow the outer disk (Kenyon & Bromley 2004). Shadowing reduces the disk luminosity and the magnitude of the IR excess. Thus, massive disks are sometimes less luminous than low mass disks (Figure 3).

Comparisons with other approaches support our estimates. Wood et al. (2002) assume the disk mass decreases homologously with time and derive IR excesses from detailed radiative transfer calculations. Their predictions for $10\ \mu\text{m}$ excesses, $\lesssim 2$ mag for disks with $\lesssim 10^{24}$ g in 1 – $100\ \mu\text{m}$ particles at 0.2 – 2 AU, agree with our results.

4. SUMMARY

Our calculations yield the first demonstration that terrestrial planet formation produces observable amounts of dust. The $10\ \mu\text{m}$ excesses range from ~ 2 mag at $t \sim 10^5$ yr to $\lesssim 0.25$ mag at $t \sim 10^6$ yr. The excesses are largest when 1000–2000 km objects form; IR excesses fade as protoplanets collide and begin to merge into Earth-mass planets.

The size and duration of IR excesses from terrestrial planet formation are similar to values needed to explain objects in transition from the opaque disks of pre-main-sequence stars to optically thin debris disks. Our models yield maximum IR excesses of $N-N_0 \approx 2$ and $Q-Q_0 \approx 3-4$; T Tauri stars with disks have $N-N_0 \approx 2-5$ and $Q-Q_0 \approx 4-8$. In $\sim 10^6$ yr, the model IR excesses decline to values consistent with those of T Tauri stars without opaque disks, $N-N_0 \lesssim 0.4$ and $Q-Q_0 \lesssim 0.5$. IR excesses probably remain at this level for $\sim 1 - 10 \times 10^7$ yr, as terrestrial planet formation concludes.

Quantifying IR excesses from 300 K dust around 1–100 Myr old solar-type stars tests predictions for dust masses and timescales for the formation of 1000–3000 km protoplanets. The models predict observable 10–20 μm excesses for $\lesssim 1$ Myr old stars and small excesses for older stars. Current ground-based 10–20 μm data agree with this prediction (e.g., Weinberger et al. 2003). Data from *SIRTF* should provide better statistics on IR excesses and a better test of the model. During the final accumulation phase, IR excesses are too small for detection with direct imaging observations. However, instruments with adaptive optics on 10–100 m class telescopes can resolve the radial dust distribution and provide direct constraints on the late epochs of terrestrial planet formation. For terrestrial planets forming around 1–10 Myr old stars, we expect dusty structures on 0.1–1 AU scales (see also Ozernoy et al. 2000), roughly similar to the 10–100 AU structures observed in debris disks around nearby A-type stars (e.g. Jayawardhana et al. 1998; Schneider et al. 1999; Weinberger et al. 1999; Wilner et al. 2002). Direct detections of these structures around nearby solar-type stars would provide good evidence for recent formation of terrestrial planets.

We acknowledge a generous allotment, ~ 1250 cpu days, of computer time at the super-computing center at the Jet Propulsion Laboratory through funding from the NASA Offices of Mission to Planet Earth, Aeronautics, and Space Science. Advice and comments from M. Geller, A. Weinberger, and the referee improved our presentation. The *NASA Astrophysics Theory Program* supported part of this project through grant NAG5-13278.

REFERENCES

- Adachi, I., Hayashi, C., & Nakazawa, K. 1976, *Progress of Theoretical Physics* 56, 1756
- Adams, F. C., Lada, C.J., & Shu, F. H. 1987, *ApJ*, 308, 788
- Adams, F. C., & Watkins, R. 1995, *ApJ*, 451, 314
- Agnor, C. B., & Ward, W. R. 2002, *ApJ*, 567, 579
- D'Alessio, P., Calvet, N., & Hartmann, L. 2001, *ApJ*, 553, 221
- Bertout, C., Basri, G., & Bouvier, J. 1988, *ApJ*, 330, 350
- van Boekel, R., Waters, L. B. F. M., Dominik, C., Bouwman, J., de Koter, A., Dullemond, C. P., & Paresce, F. 2003, *A&A*, 400, L21
- Bontemps, S. et al. 2001, *A&A*, 372, 173
- Bromley, B., & Kenyon, S. J. 2004, in preparation
- Chambers, J. E. 2001, *Icarus*, 152, 205
- Chiang, E.I., & Goldreich, P. 1999, *ApJ*, 519, 279
- Davis, D. R., Chapman, C. R., Weidenschilling, S. J., & Greenberg, R. 1985, *Icarus*, 62, 30
- Dominik, C., & Decin, G. 2004, *ApJ*, in press (astro-ph/0308364)
- Goldreich, P., & Ward, W. R. 1973, *ApJ*, 183, 1051
- Greaves, J. S., & Wyatt, M. C. 2003, *MNRAS*, in press
- Habing, H. J., et al. 2001, *A&A*, 365, 545
- Haghighipour, N., & Boss, A. P. 2003, *ApJ*, 583, 996
- Haisch, K. E., Jr., Lada, E. A., Piña, R. K.; Telesco, C. M., & Lada, C. J. 2001, *AJ*, 121, 1512
- Haisch, K., Lada, E. A., & Lada, C. J. 2001, *ApJ*, 553, L153
- Hartigan, P., Hartmann, L., Kenyon, S. J., Strom, S. E., & Skrutskie, M. F. 2001, *ApJL*, 354, L25
- Hayashi, C. 1981, *Prog Theor Phys Suppl*, 70, 35
- Hogerheijde, M. R., Johnstone, D., Matsuyama, I., Jayawardhana, R., Muzerolle, J. 2003, *ApJ*, 593, L101
- Hollenbach, D. J., Johnstone, D., Lizano, S., & Shu, F. 1994, *ApJ*, 428, 654
- Jayawardhana, R. et al. 1998, *ApJ*, 503, L79
- Jayawardhana, R., Wolk, S. J., Barrado y Navascués, D., Telesco, C. M., & Hearty, T. J. 2001, *ApJ*, 550, L197
- Lagrange, A.-M., Backman, D., & Artymowicz, P. 2000, in *Protostars & Planets IV*, eds. V. Mannings, A. P. Boss, & S. S. Russell, Tucson, Univ. of Arizona, p. 639
- Kenyon, S. J., & Bromley, B. C. 2001, *AJ*, 121, 538
- Kenyon, S. J., & Bromley, B. C., 2002a, *AJ*, 123, 1757
- Kenyon, S. J., & Bromley, B. C. 2002b, *ApJ*, 577, L35

- Kenyon, S. J., & Bromley, B. C., 2004, *AJ*, 127, No. 1
- Kenyon, S. J., & Hartmann, L. 1987, *ApJ*, 323, 714
- Kenyon, S. J., & Hartmann, L. 1995, *ApJS*, 101, 117
- Kenyon, S. J., & Luu, J. X. 1998, *AJ*, 115, 2136
- Kenyon, S. J., & Luu, J. X. 1999, *AJ*, 118, 1101
- Kenyon, S. J., Wood, K., Whitney, B. A., & Wolff, M. 1999, *ApJ*, 524, L119
- Konigl, A., & Pudritz, R. 2000, 2000, in *Protostars & Planets IV*, eds. V. Mannings, A. P. Boss, & S. S. Russell, Tucson, Univ. of Arizona, 759
- Lissauer, J. J. 1987, *Icarus*, 69, 249
- Lissauer, J. J. 1993, *ARA&A*, 31, 129
- Lynden-Bell, D., & Pringle, J. E. 1974, *MNRAS*, 168, 603
- Najita, J., Carr, J. S., & Mathieu, R. D. 2003, *ApJ*, 589, 931
- Ohtsuki, K., Stewart, G. R., & Ida, S. 2002, *Icarus*, 155, 436
- Ozernoy, L. M., Gorkabyi, N. N., Mather, J. C., & Taidakova, T. A. 2000, *ApJ*, 537, L147
- Pollack, J. B., Hubickyj, O., Bodenheimer, P., Lissauer, J. J., Podolak, M., & Greenzweig, Y. 1996, *Icarus*, 124, 62
- Rafikov, R. R. 2001, *AJ*, 122, 2713
- Rafikov, R. R. 2003, *AJ*, 126, 2529
- Rucinski, S. M. 1985, *AJ*, 90, 2321
- Safronov, V. S. 1969, *Evolution of the Protoplanetary Cloud and Formation of the Earth and Planets*, Nauka, Moscow [Translation 1972, NASA TT F-677]
- Schneider, G., et al. 1999, *ApJ*, 513, L127
- Spangler, C., Sargent, A. I., Silverstone, M. D., Becklin, E. E., & Zuckerman, B. 2001, *ApJ*, 555, 932
- Stassun, K. G., M., Robert D., Vrba, F. J., Mazeh, T., & Henden, A. 2001, *AJ*, 121, 1003
- Supulver, K. D., & Lin, D. N. C. 2000, *Icarus*, 146, 525
- Throop, H. B., Bally, J., Esposito, L. W., & McCaughrean, M. J. 2001, *Science*, 292, 1686
- Weidenschilling, S. J. 1977, *Ap Sp Sci*, 51, 153
- Weidenschilling, S. J., & Cuzzi, J. N., 1993, in *Protostars and Planets III*, ed. E. H. Levy & J. I. Lunine (Tucson: Univ of Arizona), p. 1031
- Weidenschilling, S. J., Spaute, D., Davis, D. R., Marzari, F., & Ohtsuki, K. 1997, *Icarus*, 128, 429
- Weinberger, A. J., Becklin, E. E., Zuckerman, B., Song, I. 2003, *BAAS*, 202, 3401
- Weinberger, A. J., Becklin, E. E., Schneider, G., Smith, B. A., Lowrance, P. J., Silverstone, M. D., Zuckerman, B., Terrile, R. J. 1999, *ApJ*, 525, L53
- Wetherill, G. W., & Stewart, G. R. 1993, *Icarus*, 106, 190
- Williams, D. R., & Wetherill, G. W. 1994, *Icarus*, 107, 117
- Wilner, D. J., Holman, M. J., Kuchner, M. J., & Ho, P. T. P. 2002, *ApJ*, 569, 115

- Wood, K., Lada, C. J., Bjorkman, J. E., Kenyon, S. J., Whitney, B., Wolff, M. J. 2002, ApJ, 567, 1183
- Wyatt, M. C., Dent, W. R. F., & Greaves, J. S. 2003, MNRAS, 342, 867
- Youdin, A. N., & Shu, F. H. 2002, ApJ, ApJ, 580, 494

Figure Captions

Fig. 1 – Masses of the largest objects for a thin torus model with $\Sigma_0 = 16 \text{ g cm}^{-2}$ and Wetherill & Stewart (1993) fragmentation. (a) lower panel: $t = 10^5 \text{ yr}$; (b) upper panel: $t = 10^6 \text{ yr}$. The horizontal error bars indicate the extent of the orbit for each object.

Fig. 2 – Evolution of the dust mass in small grains ('S'; $1 \mu\text{m} \leq r \leq 1 \text{ m}$) and large grains ('L'; $1 \text{ mm} \leq r \leq 1 \text{ m}$) for models with Σ_0 as indicated in the legend. More massive disks produce more debris at earlier times than less massive disks. For all disks, the dust production rate converges to a power-law decline with time.

Fig. 3 – Evolution of the broadband $10 \mu\text{m}$ (N-N₀) and $20 \mu\text{m}$ (Q-Q₀) excesses as a function of time. Left panels: 0.84–1.16 AU torus calculations; right panels: 0.68–1.32 AU torus calculations. Fragmentation produces large excesses relative to a stellar photosphere at $t \sim 10^4$ to 10^5 yr . By $t \sim 10^6 \text{ yr}$, the $10 \mu\text{m}$ excess is nearly unobservable; a small excess persists at $20 \mu\text{m}$.

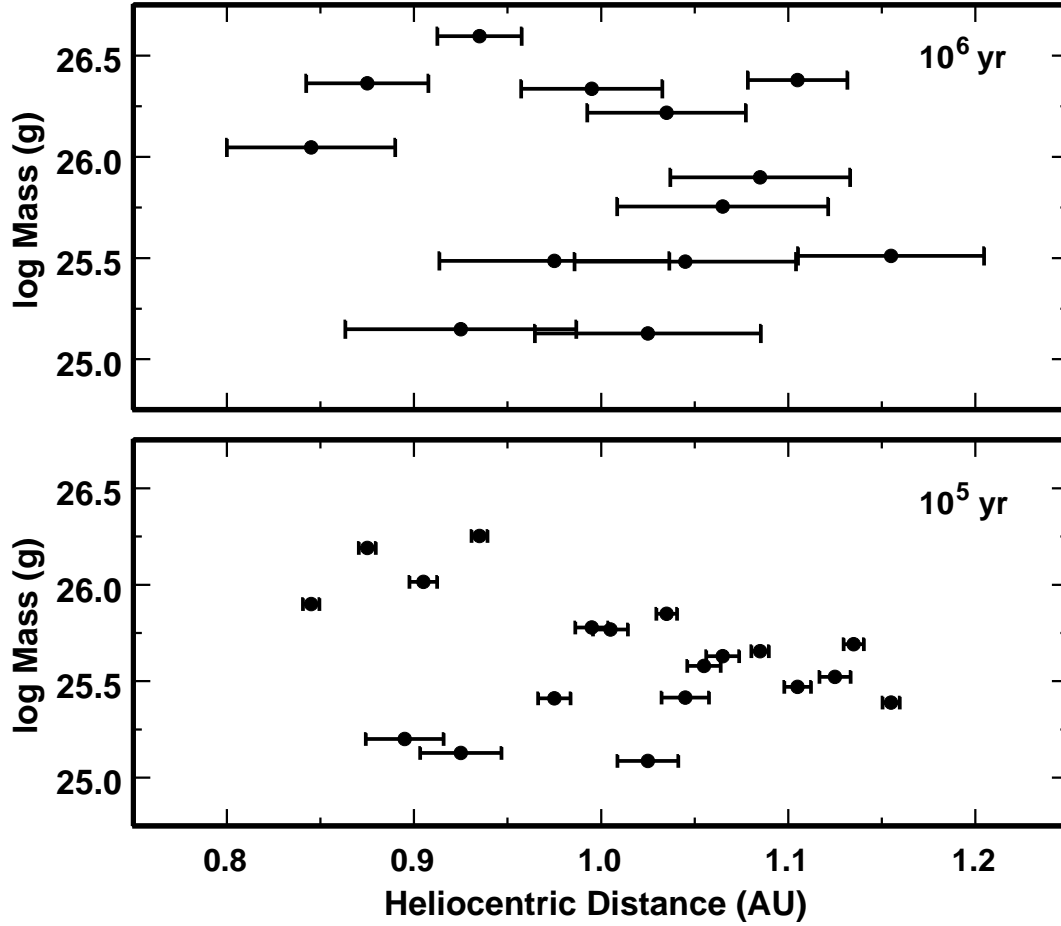


Fig. 1.— Masses of the largest objects for a thin torus model with $\Sigma_0 = 16 \text{ g cm}^{-2}$ and Wetherill & Stewart (1993) fragmentation. (a) lower panel: $t = 10^5 \text{ yr}$; (b) upper panel: $t = 10^6 \text{ yr}$. The horizontal error bars indicate the extent of the orbit for each object.

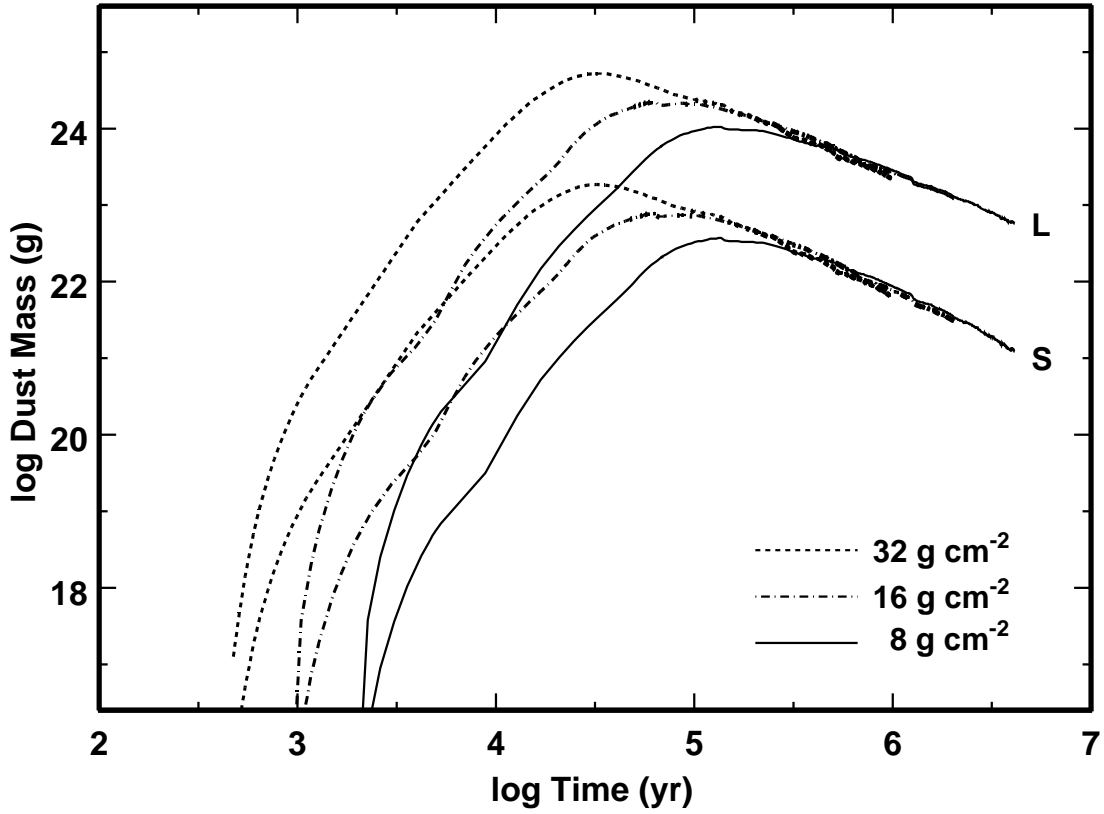


Fig. 2.— Evolution of the broadband $10 \mu\text{m}$ ($N-N_0$) and $20 \mu\text{m}$ ($Q-Q_0$) excesses as a function of time. Left panels: 0.84–1.16 AU torus calculations; right panels: 0.68–1.32 AU torus calculations. Fragmentation produces large excesses relative to a stellar photosphere at $t \sim 10^4$ to 10^5 yr. By $t \sim 10^6$ yr, the $10 \mu\text{m}$ excess is unobservable; a small excess persists at $20 \mu\text{m}$.

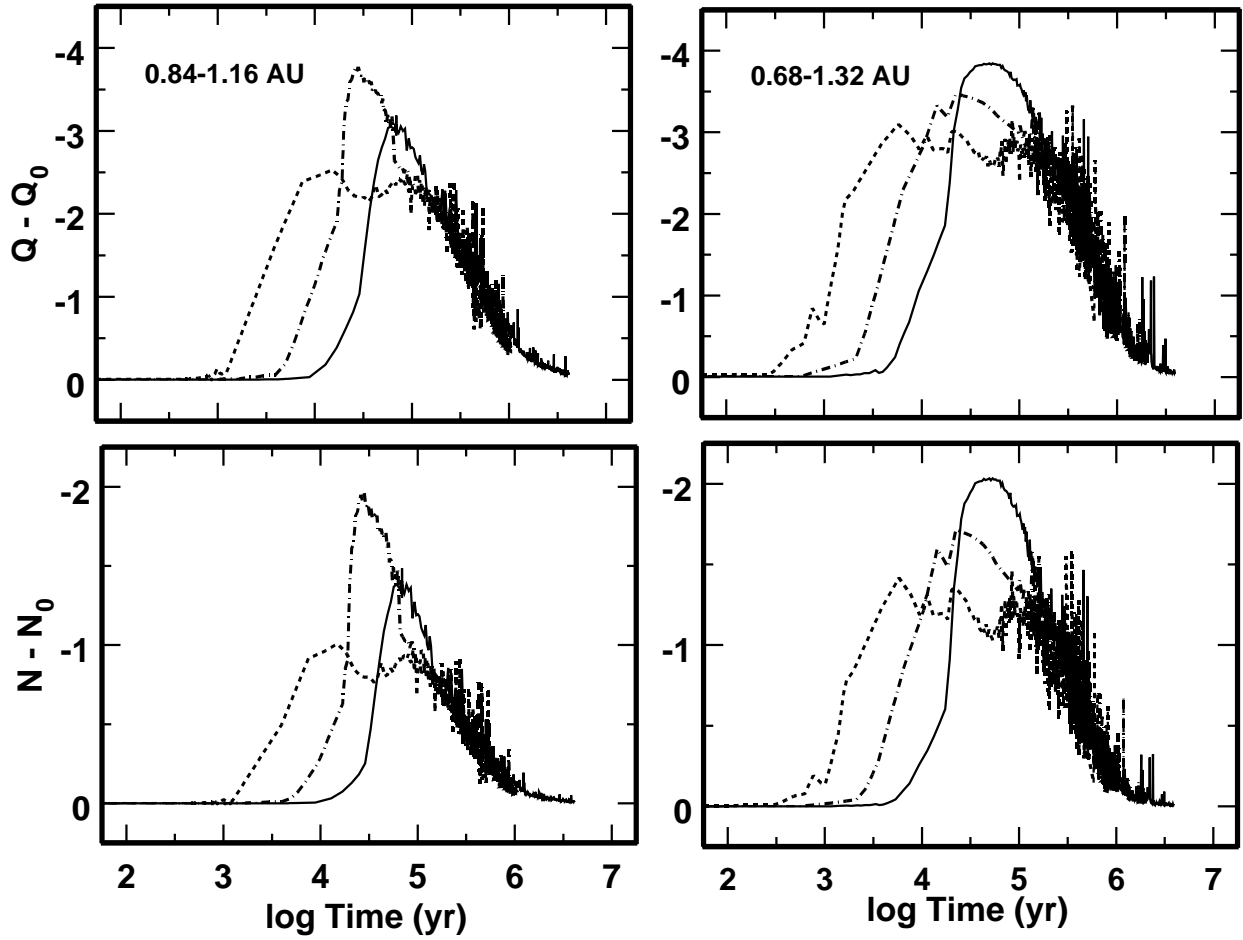


Fig. 3.— Evolution of the broadband $10 \mu\text{m}$ ($N - N_0$) and $20 \mu\text{m}$ ($Q - Q_0$) excesses as a function of time. Left panels: 0.84–1.16 AU torus calculations; right panels: 0.68–1.32 AU torus calculations. Fragmentation produces large excesses relative to a stellar photosphere at $t \sim 10^4$ to 10^5 yr. By $t \sim 10^6$ yr, the $10 \mu\text{m}$ excess is nearly unobservable; a small excess persists at $20 \mu\text{m}$.